

TASK コードによるアルヴェン固有モードの解析

京大工：福山 淳

内 容

- 目 的
- アルヴェン固有モード 解析
- まとめ

目的

- トカマクにおける多様なアルヴェン固有モード
 - CAE : 圧縮性アルヴェン固有モード (高周波数 , 球状トカマク)
 - EAE : Ellipticity-induced Alfvén eigenmode (楕円断面)
 - TAE : Toroidicity-induced Alfvén eigenmode (トーラスプラズマ)
 - GAE : Global Alfvén eigenmode (円柱プラズマ)
 - EPM, RSAE, BAE : Energetic Particle Driven mode (高速イオン)
 - DAE : Drift-Alfvén eigenmode (ドリフト波との結合)
- 負磁気シア配位におけるアルヴェン固有モード
 - TAE 安定化の予測 : アルヴェン共鳴による吸収の増加 (Nova-K)
 - 周波数が大幅に変化する固有モードの存在 (JT-60U, JET)

アルヴェン固有モードの線形安定性解析

- 電磁流体的解析（理想，抵抗性）
- 運動論的効果を含めた電磁流体的解析（摂動的）
 - 固有関数は電磁流体方程式から。運動論的効果を含めて成長率を評価。
- 運動論的解析（電子の質量，イオンの有限半径，ドリフト運動等）
 - PENN code (Jaun, Alfvén Lab)
 - TASK/WM (Fukuyama)
- バルーニング展開（高 n モード）
 - HINST (Gorelenkov, Cheng)
 - 2D-WKB (Vlad, Chen, Zonka)
- 3次元波動伝播解析コード TASK/WM
 - MHD 平衡解析から得られる磁気面座標
 - マクスウェル方程式の境界値問題。プラズマの応答は誘電率テンソル
 - ポロイダル方向とトロイダル方向にはフーリエモード展開，径方向には差分
 - 一定振幅の励起に対して振幅が最大となる複素固有周波数を求める。

磁気面座標

- 磁気面座標(非直交座標系)

- 小半径方向: ポロイダル磁束 ψ
- ポロイダル方向: θ
- トロイダル方向: φ

- 反変基本ベクトル

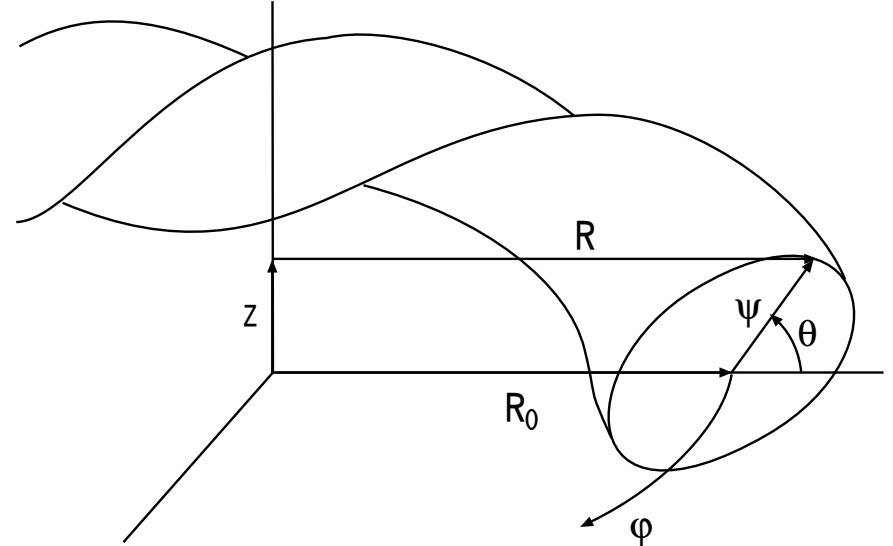
$$e^1 = \nabla\psi, \quad e^2 = \nabla\theta, \quad e^3 = \nabla\varphi$$

を用いると、電界ベクトルは

$$\mathbf{E} = E_1 e^1 + E_2 e^2 + E_3 e^3$$

- J : ヤコビアン
$$J = \frac{1}{e^1 \cdot e^2 \times e^3} = \frac{1}{\nabla\psi \cdot \nabla\theta \times \nabla\varphi}$$

- g : 計量係数 共変基本ベクトル $e_i \equiv \partial r / \partial x_i$ を用いて $g_{ij} = e_i \cdot e_j$



波動方程式

- 波動電界 E に対する定常マクスウェル方程式(角周波数 ω , 光速 c)

$$\nabla \times \nabla \times E = \frac{\omega^2}{c^2} \overset{\leftrightarrow}{\epsilon} \cdot E + i\omega\mu_0 j_{\text{ext}}$$

- $\overset{\leftrightarrow}{\epsilon}$: 誘電率テンソル [有限温度効果(サイクロトロン減衰 , ランダウ減衰)]
- j_{ext} : アンテナ電流

- 非直交座標系における波動方程式(半径方向成分)

$$(\nabla \times \nabla \times E)^1 = \frac{1}{J} \left[\frac{\partial}{\partial x^2} \left\{ \frac{g_{31}}{J} \left(\frac{\partial E_3}{\partial x^2} - \frac{\partial E_2}{\partial x^3} \right) + \frac{g_{32}}{J} \left(\frac{\partial E_1}{\partial x^3} - \frac{\partial E_3}{\partial x^1} \right) + \frac{g_{33}}{J} \left(\frac{\partial E_2}{\partial x^1} - \frac{\partial E_1}{\partial x^2} \right) \right\} \right.$$
$$\left. - \frac{\partial}{\partial x^3} \left\{ \frac{g_{21}}{J} \left(\frac{\partial E_3}{\partial x^2} - \frac{\partial E_2}{\partial x^3} \right) + \frac{g_{22}}{J} \left(\frac{\partial E_1}{\partial x^3} - \frac{\partial E_3}{\partial x^1} \right) + \frac{g_{23}}{J} \left(\frac{\partial E_2}{\partial x^1} - \frac{\partial E_1}{\partial x^2} \right) \right\} \right]$$

- (x^1, x^2, x^3) はそれぞれ座標 (ψ, θ, φ) を表す .
- ポロイダル成分とトロイダル成分も同様

プラズマ応答

- 誘電率テンソル $\overset{\leftrightarrow}{\epsilon}$ は，通常静磁界を z 軸とする規格化直交座標系で記述
- 局所的な規格化直交座標系 $\hat{e}_s = \frac{\nabla \psi}{|\nabla \psi|}, \quad \hat{e}_b = \hat{e}_h \times \hat{e}_\psi, \quad \hat{e}_h = \frac{\mathbf{B}_0}{|\mathbf{B}_0|}$
- 座標変換行列 : $\overset{\leftrightarrow}{\mu}$

$$\begin{pmatrix} E_1 \\ E_2 \\ E_3 \end{pmatrix} = \overset{\leftrightarrow}{\mu} \begin{pmatrix} E_s \\ E_b \\ E_h \end{pmatrix}$$

$$\overset{\leftrightarrow}{\mu} \equiv \begin{pmatrix} \frac{1}{\sqrt{g^{11}}} & \frac{d}{\sqrt{Jg^{11}}} & c_2 g_{12} + c_3 g_{13} \\ 0 & c_3 J \sqrt{g^{11}} & c_2 g_{22} + c_3 g_{23} \\ 0 & -c_2 J \sqrt{g^{11}} & c_2 g_{32} + c_3 g_{33} \end{pmatrix} \quad \begin{aligned} c_2 &= B^\theta / B, & c_3 &= B^\phi / B \\ d &= c_2(g_{23}g_{12} - g_{22}g_{31}) + c_3(g_{33}g_{12} - g_{32}g_{31}) \\ g^{11} &= (g_{22}g_{33} - g_{23}g_{32}) / J^2 \end{aligned}$$

- 非直交座標系における誘電テンソル

$$\overset{\leftrightarrow}{\epsilon} = \overset{\leftrightarrow}{\mu} \cdot \overset{\leftrightarrow}{\epsilon}_{sbh} \cdot \overset{\leftrightarrow}{\mu}^{-1}$$

フーリエ展開

- ポロイダル方向とトロイダル方向については，フーリエ級数により展開
- 電界，マクスウェル方程式の左辺，形状および媒質の変化を表す係数をそれぞれ

$$E(\psi, \theta, \varphi) = \sum_{mn} E_{mn}(\psi) e^{i(m\theta + n\varphi)}$$

$$G(\psi, \theta, \varphi) = \sum_{lk} G_{lk}(\psi) e^{i(l\theta + kN_p\varphi)}$$

$$J(\nabla \times \nabla \times \mathbf{E}) = G(\psi, \theta, \varphi) E(\psi, \theta, \varphi) = \sum_{m'n'} [J(\nabla \times \nabla \times \mathbf{E})]_{m'n'} e^{i(m'\theta + n'\varphi)}$$

- モード間結合 (N_h : トロイダル方向のヘリカルコイル回転数)

モード番号	トロイダル方向	ポロイダル方向
電界ベクトル E	n	m
媒質変化	kN_h	l
$J(\nabla \times \nabla \times \mathbf{E})$	n'	m'
関係式	$n' = n + kN_h$	$m' = m + l$

平行方向の波数

- プラズマ誘電テンソル $\overset{\leftrightarrow}{\epsilon}(\psi, \theta, \varphi, k_{\parallel}^{m''n''})$ は、
 プラズマ分散関数 $Z[(\omega - N\omega_{\text{cs}})/k_{\parallel}^{m''n''}v_{\text{Ts}}]$ を通して、
 磁力線方向の波数 $k_{\parallel}^{m'',n''}$ に依存する。

$$k_{\parallel}^{m'',n''} = -i\hat{\mathbf{e}}_h \cdot \nabla = -i\hat{\mathbf{e}}_h \cdot (\nabla\theta \frac{\partial}{\partial\theta} + \nabla\varphi \frac{\partial}{\partial\varphi}) = -i\hat{\mathbf{e}}_h \cdot (\mathbf{e}^2 \frac{\partial}{\partial\theta} + \mathbf{e}^3 \frac{\partial}{\partial\varphi}) = m'' \frac{B^\theta}{|B|} + n'' \frac{B^\varphi}{|B|}$$

- 誘電テンソル $\overset{\leftrightarrow}{\epsilon}_{sbh}$ に対応する電界のフーリエ成分

$$(J \overset{\leftrightarrow}{\epsilon} \cdot \mathbf{E})^i = J \overset{\leftrightarrow}{g}^{-1} \cdot \overset{\leftrightarrow}{\mu} \cdot \overset{\leftrightarrow}{\epsilon}_{sbh} \cdot \overset{\leftrightarrow}{\mu}^{-1} \cdot \mathbf{E}_i$$

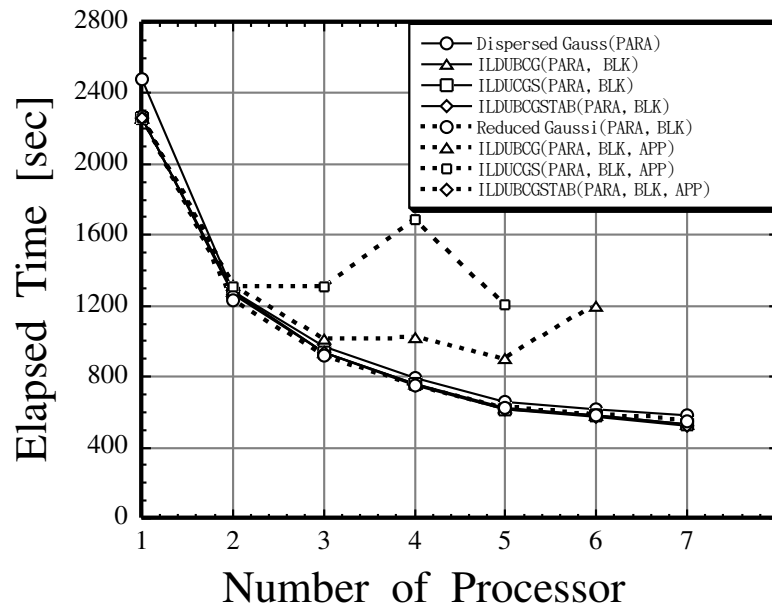
m'	ℓ_3	ℓ_2	ℓ_1	m
n'	k_3	k_2	k_1	n

したがって

$$\begin{aligned} m'' &= m + \ell_1 + \frac{1}{2}\ell_2 & n'' &= n + k_1 + \frac{1}{2}k_2 \\ m' &= m + \ell_1 + \ell_2 + \ell_3 & n' &= n + k_1 + k_2 + k_3 \end{aligned}$$

並列処理による TASK/WM の高速化

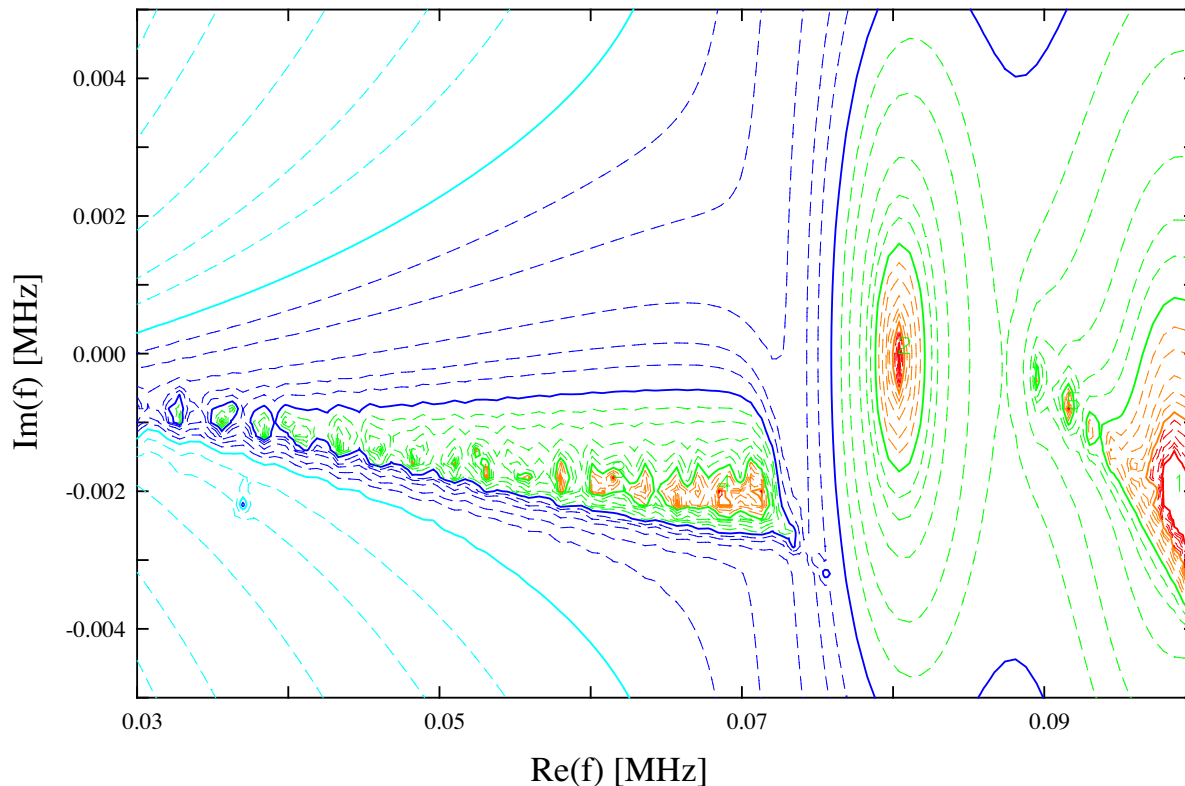
- 計算機クラスターによる並列処理 (Fortran77 + MPI ライブラリ)
 - 並列処理による係数行列計算の高速化
 - 並列処理による行列方程式解法の高速化
 - 係数配列の分散記憶による大規模化
- 経過時間のプロセッサ数依存性 (16 モード , 径方向 50 点)



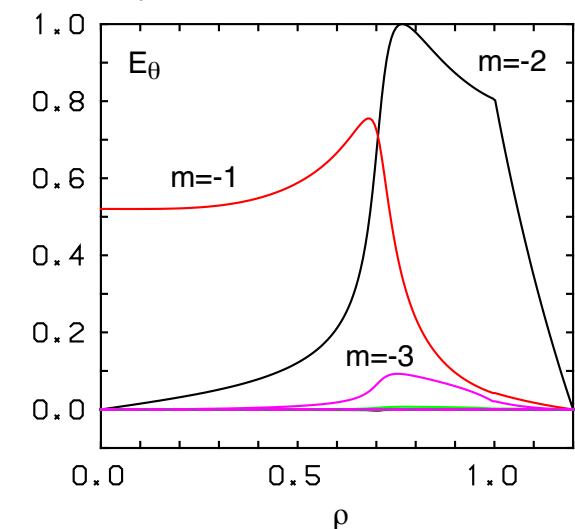
正磁気シア : TAE

- $q(\rho) = q_0 + (q_a - q_0)\rho^2$, $q_0 = 1$, $q_a = 2$
- 平坦密度分布

複素周波数空間における振幅等高線



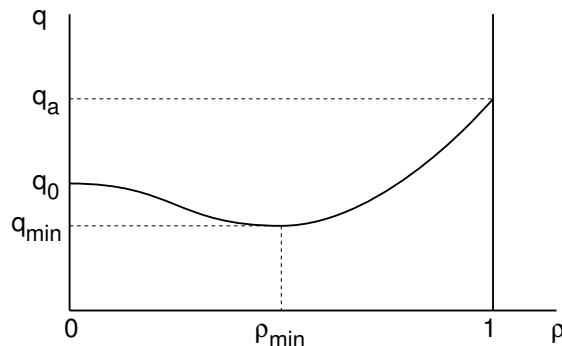
$$f_r = 81.95 \text{ kHz}$$
$$f_i = -20.32 \text{ Hz}$$



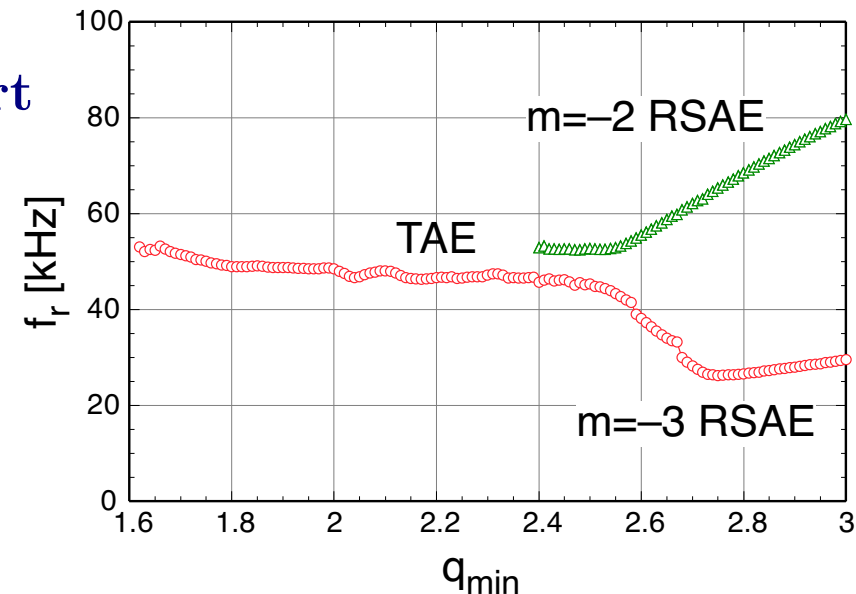
Analysis of TAE in Reversed Shear Configuration

q_{\min} Dependence of Eigenmode Frequency

Assumed q profile



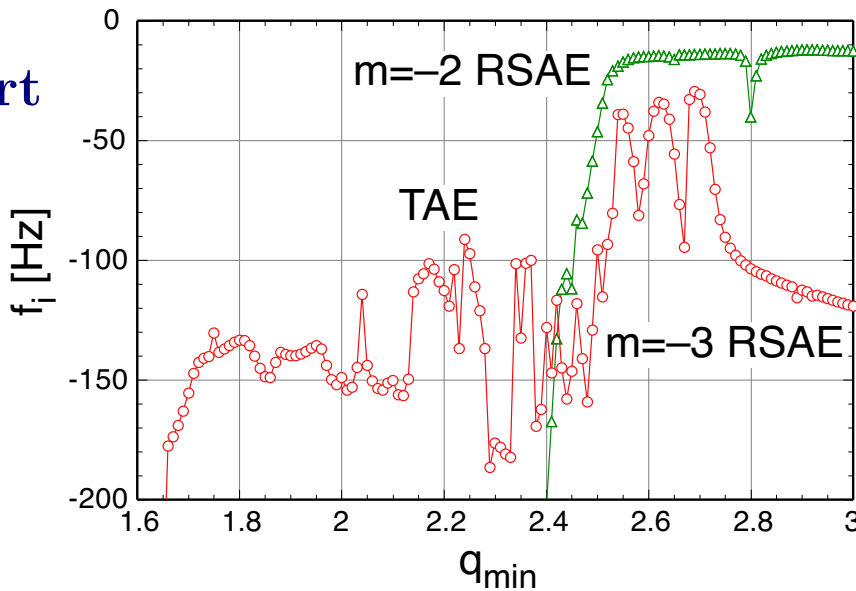
Real part



Plasma Parameters

R_0	3 m
a	1 m
B_0	3 T
$n_e(0)$	10^{20} m^{-3}
$T(0)$	3 keV
$q(0)$	3
$q(a)$	5
ρ_{\min}	0.5
n	1
Flat density profile	

Imag part



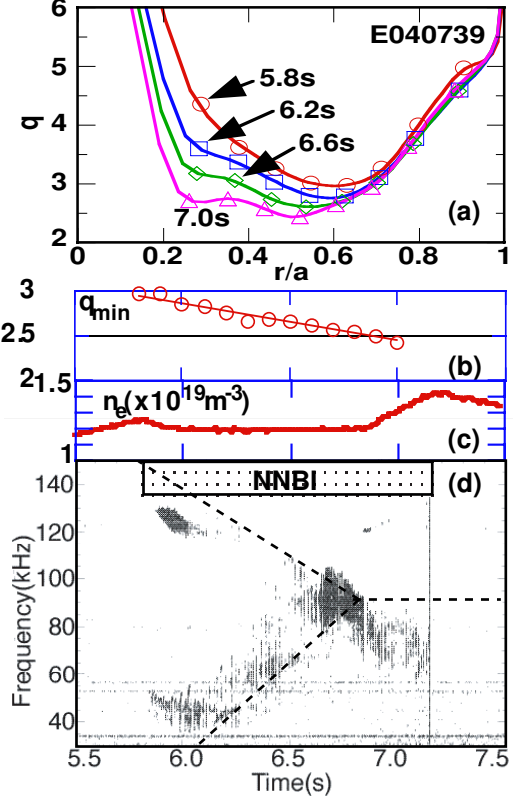


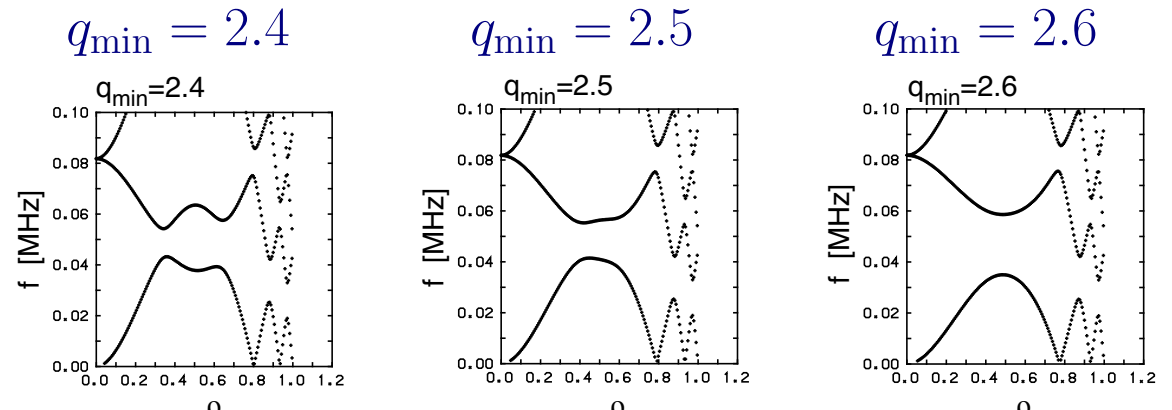
FIG. 1: (a) Temporal evolution of the q -profile measured with MSE. (b) Temporal evolution of q_{\min} , (c) line averaged electron density, (d) a typical behavior of frequency spectrum of the $n = 1$ AE. Broken lines denote estimated frequency from the RSAE model normalized by observed frequency at $q = 2.5$.

probes separated by about 40 degree in the toroidal direction is larger than 0.9. the only $n = 1$ AE is observed because β_h is relatively low ($\beta_h < 0.2\%$). AEs with $n > 1$ are observed if β_h increases. The large upward/downward frequency sweeping from $t = 6.0$ – 6.5 s cannot be explained by the change of V_A because the electron density changed only less than 5%. In the period $t = 6.5$ – 6.8 s the $n = 1$ AE frequency saturates. After $t \sim 6.8$ s the $n = 1$ AE frequency decreases due to the increase of electron density.

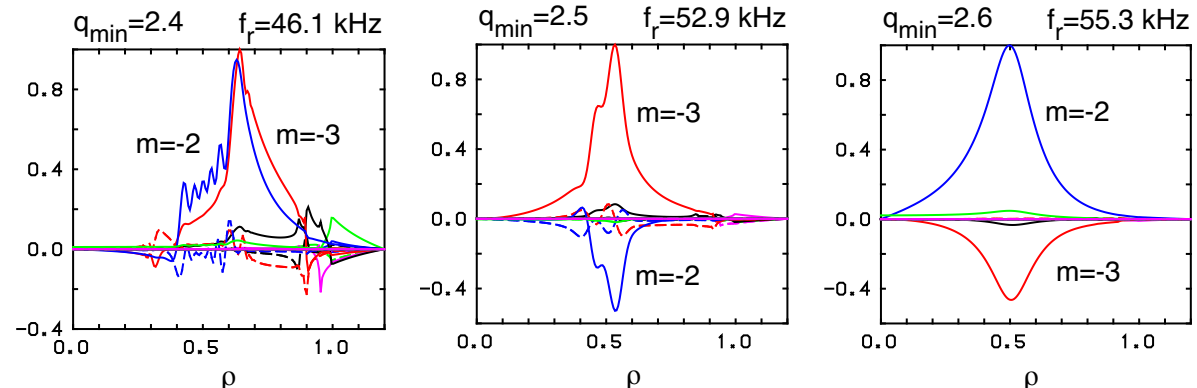
The observed AE amplitude are enhanced during $t \approx 6.65$ – 6.85 s when the AE frequency is saturated as shown in Fig. 1(d). To investigate the dependence of mode amplitude on the q -profile change, we show the mode amplitude versus q_{\min} for three shots in Fig. 2. When NNBI was injected the values of q_{\min} are about 3.0, 2.8 and 2.6 for the shots of E40739, E40744 and E40743, respectively. For all these cases the $n = 1$ mode amplitude is largest

負磁気シア配位における固有モード構造

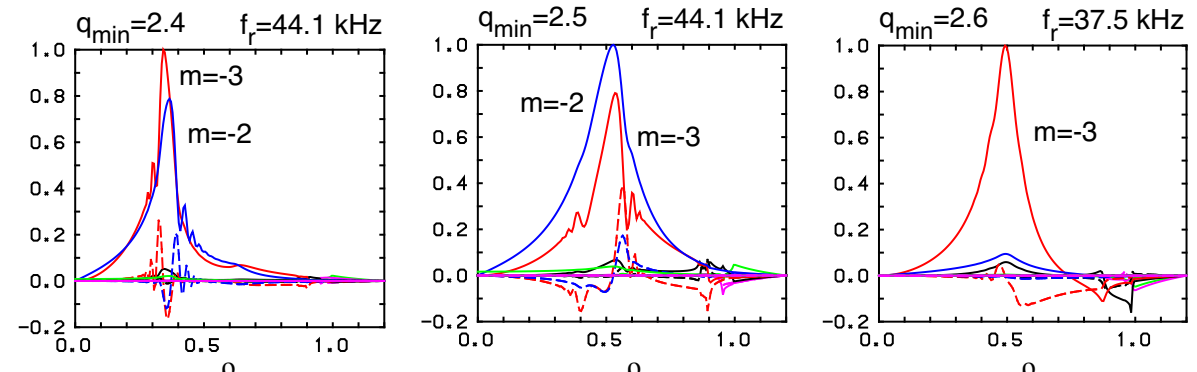
Alfvén resonance



Higher freq.



Lower freq.



TAEs

Double TAE

RSAE

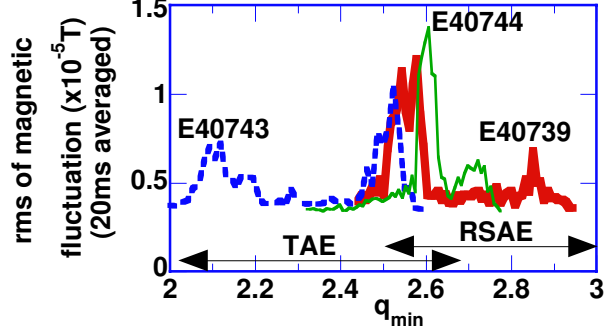


FIG. 2: Dependence of AE magnetic fluctuation amplitude on q_{\min} . The $n = 1$ AE amplitude is enhanced in the range of $2.4 < q_{\min} < 2.7$.

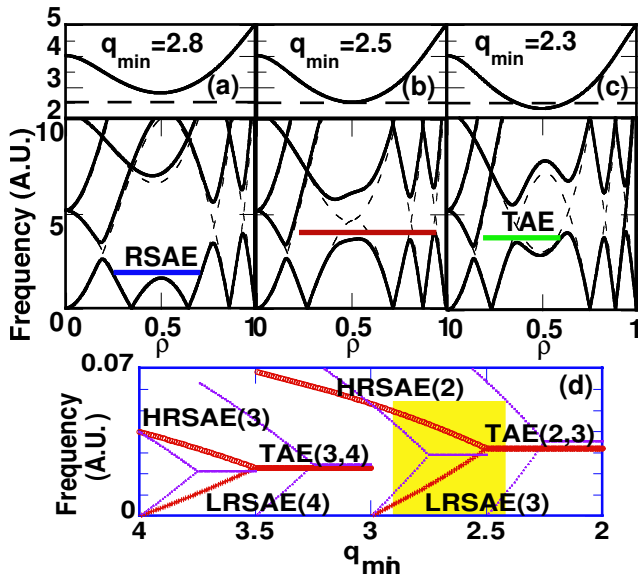


FIG. 3: Schematic drawing of the $n = 1$ spectrum of AEs in the RS plasma with (a) $q_{\min} = 2.8$, (b) $q_{\min} = 2.5$ and (b) $q_{\min} = 2.3$. Panel (d) shows the frequencies of RSAE and TAE as a function of q_{\min} . The bold lines denote the frequencies of the $n = 1$ AEs and thin lines are for the $n = 2$ AEs. Numbers in the parentheses are poloidal mode numbers.

in the range $2.4 < q_{\min} < 2.7$, which is independent of the time length after NNB injection.

To understand the large and rapid frequency sweeping and its subsequent saturation, we propose a model of RSAE and its transition to TAE as q_{\min} decreases. Fig. 3 shows three shear Alfvén continuous spectra, frequency vs. r/a , in RS plasmas with (a) $q_{\min} = 2.8$, (b) $q_{\min} = 2.5$ and (c) $q_{\min} = 2.3$. In any cases, $n = 1$, $q(0) = 3$ at the plasma center, and $q(a) = 5$ at the plasma edge. The two gaps around the q_{\min} region shown in Fig. 3(c) are

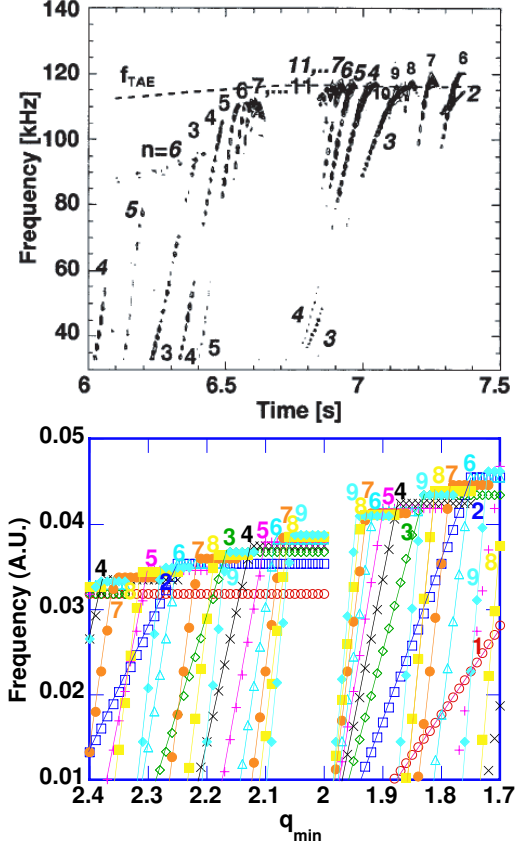
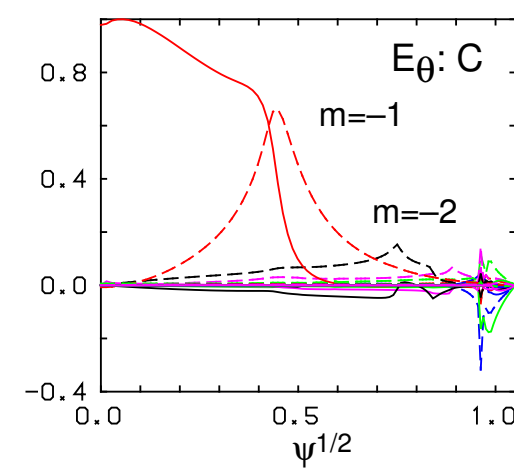
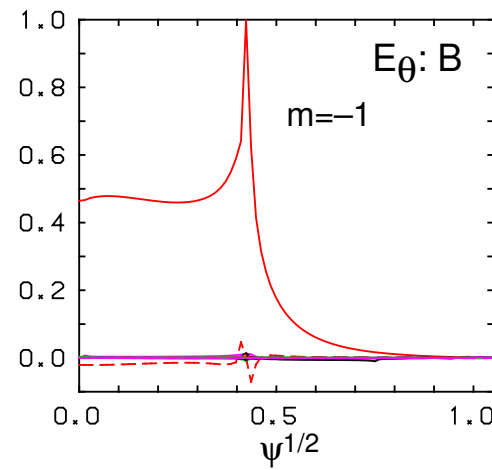
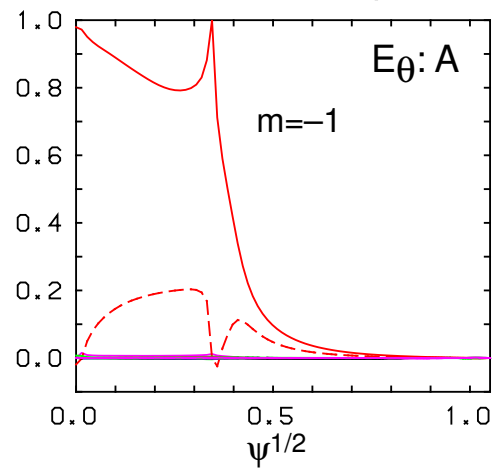
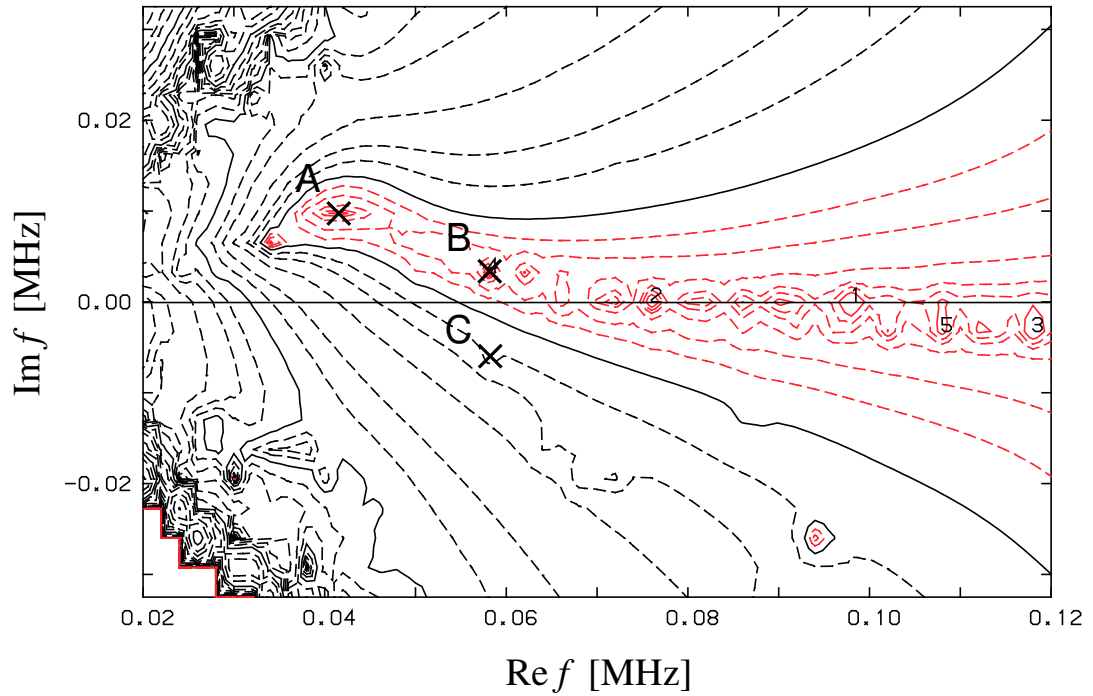
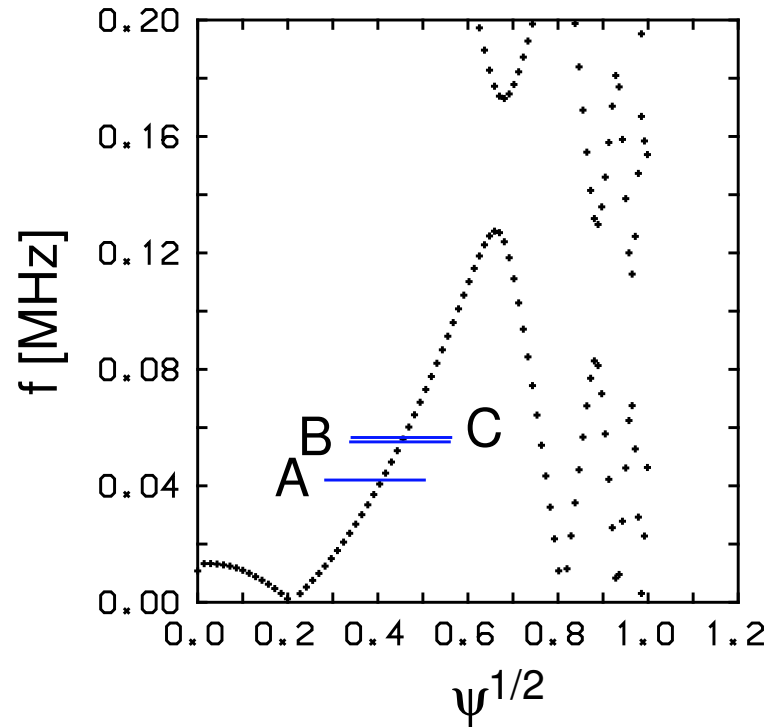


FIG. 5: (a) Typical temporal evolution of AE frequency changes observed in a JT-60U ICRF heated RS plasma [6]. (b) The frequencies of $n= 1–9$ LRSAEs (solid upward-sloping lines) and TAEs (horizontal aligned marks) as a function of the q_{\min} decrement.

assume that q_{\min} decreases in time as it does. If the modes in the experiment just trace the Alfvén dispersion relation, which is $\omega_A/V_A = |k_{\parallel}(r)| = |n - m/q(r)|/R$, at $q = q_{\min}$, and q_{\min} decrease, the frequency would increase in time when $k_{\parallel}(r_0) < 0$ and decrease in time when $k_{\parallel}(r_0) > 0$. However, the modes with downward sweeping are suppressed in the experiment. They interpret no observation of downward frequency sweeping after upward frequency sweeping by effect of energetic particles. They assert that the only way they have found to explain the asymmetry is to describe the fast particle response in a nonperturbative manner. On the other hand, from our RSAE model, there are inherently TAEs rather than modes with downward sweeping after upward sweeping, i.e., AE transits from LRSAE to TAE. We don't observe TAE after RSAE when β_h is not sufficiently large, because damping rate of TAE is larger than that of LRSAE. When β_h is sufficiently high, TAE can be destabilized in the q_{\min} transition range as observed in our NNB RS plasma

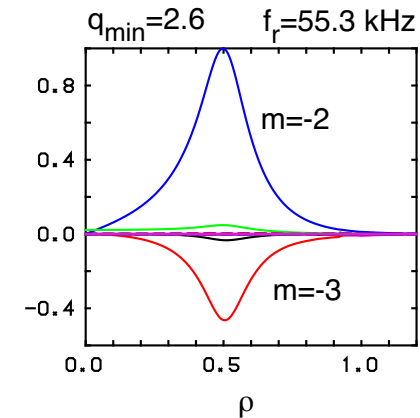
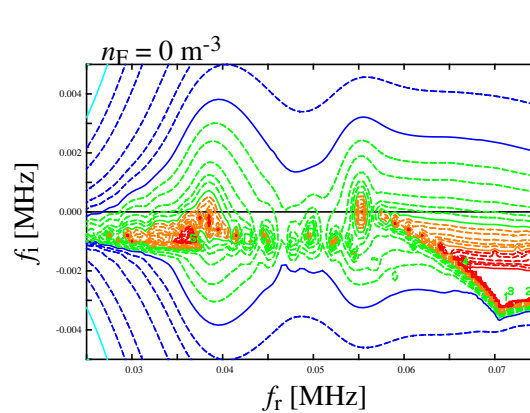
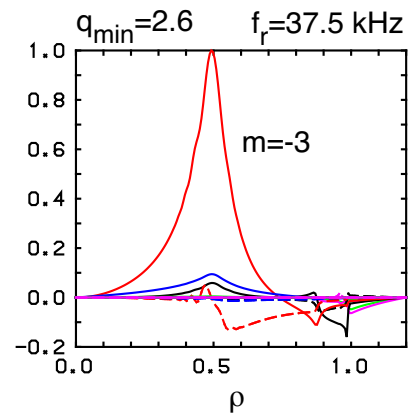
高速イオン励起モード



$$(f_r, f_i) = (41.8, 8.1) \text{ kHz} \quad (f_r, f_i) = (57.7, 3.6) \text{ kHz} \quad (f_r, f_i) = (58.0, -6.0) \text{ kHz}$$

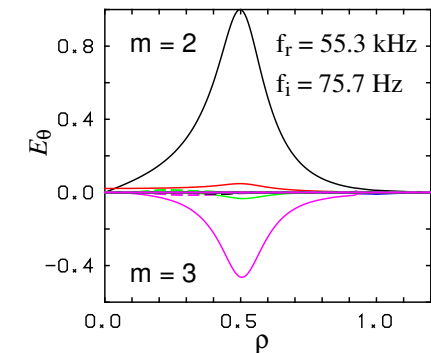
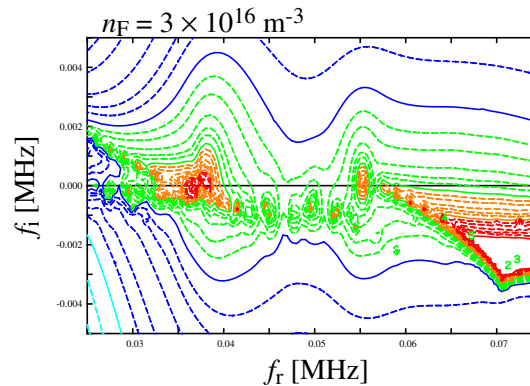
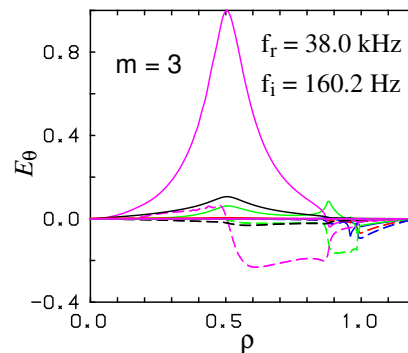
高速イオンによる RSAE の励起 ($q_{\min} = 2.6$)

- Without EP



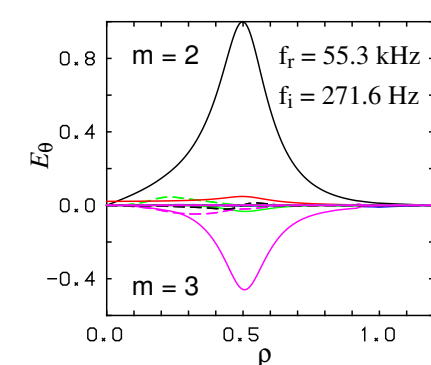
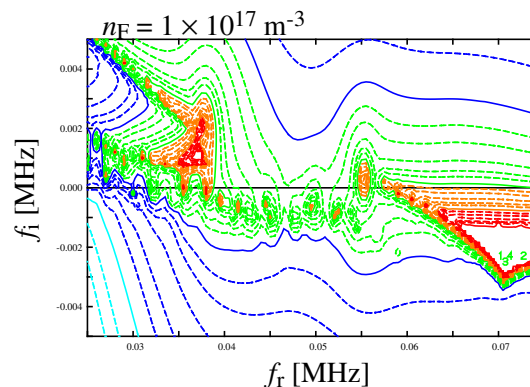
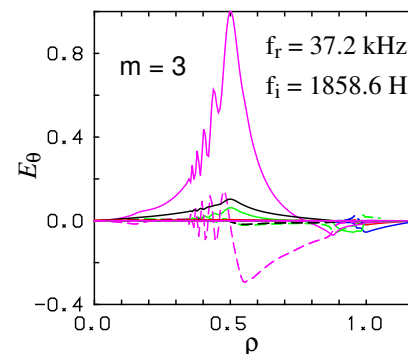
- With EP

3×10^{16} m⁻³
360 keV
0.5 m



- With EP

1×10^{17} m⁻³
360 keV
0.5 m



まとめ

- 負磁気シア配位においては，TAE はより安定となるが，周波数ギャップの上下端近傍に固有周波数をもつ固有モード RSAE が存在できる．
- RSAE は安全係数の最小値付近に局在したGAEとみなすこともできる．
- RSAE の存在範囲は おおよそ $\ell + 0.5 \lesssim q_{\min} \lesssim \ell + 0.7$ である．
- 高速イオンによるアルヴェン固有モードの不安定化を取り入れ，周波数ギャップよりも低い周波数領域の固有モードが不安定化される条件を調べた．
- 進行中
 - 高速イオンによる RSAE の不安定化
 - MHD モードの解析（阿久津）
 - 圧力勾配や電流を取り入れた流体的誘電率テンソル
 - 空間不均一性を取り入れたジャイロ運動論的誘電率テンソル
 - 有限軌道幅効果を取り入れた積分形誘電率テンソル

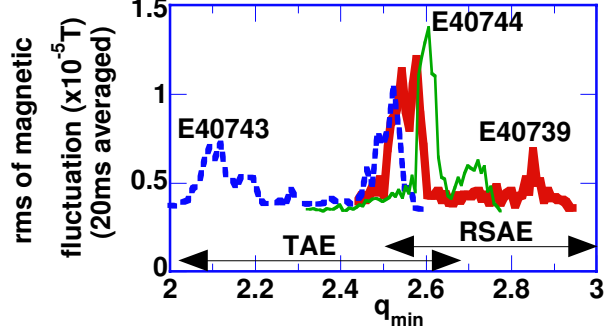


FIG. 2: Dependence of AE magnetic fluctuation amplitude on q_{\min} . The $n = 1$ AE amplitude is enhanced in the range of $2.4 < q_{\min} < 2.7$.

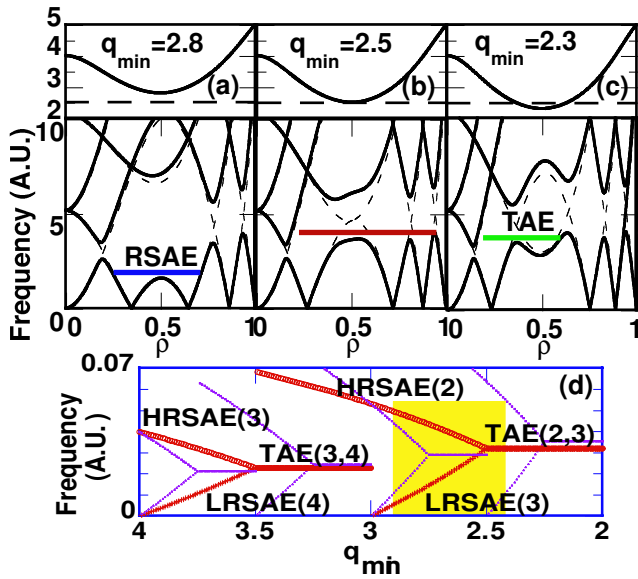


FIG. 3: Schematic drawing of the $n = 1$ spectrum of AEs in the RS plasma with (a) $q_{\min} = 2.8$, (b) $q_{\min} = 2.5$ and (b) $q_{\min} = 2.3$. Panel (d) shows the frequencies of RSAE and TAE as a function of q_{\min} . The bold lines denote the frequencies of the $n = 1$ AEs and thin lines are for the $n = 2$ AEs. Numbers in the parentheses are poloidal mode numbers.

in the range $2.4 < q_{\min} < 2.7$, which is independent of the time length after NNB injection.

To understand the large and rapid frequency sweeping and its subsequent saturation, we propose a model of RSAE and its transition to TAE as q_{\min} decreases. Fig. 3 shows three shear Alfvén continuous spectra, frequency vs. r/a , in RS plasmas with (a) $q_{\min} = 2.8$, (b) $q_{\min} = 2.5$ and (c) $q_{\min} = 2.3$. In any cases, $n = 1$, $q(0) = 3$ at the plasma center, and $q(a) = 5$ at the plasma edge. The two gaps around the q_{\min} region shown in Fig. 3(c) are